AIAA JOURNAL
Vol. 44, No. 4, April 2006

Turbulence Modeling for Very Large-Eddy Simulation

Nan-Suey Liu* and Tsan-Hsing Shih†
NASA John H. Glenn Research Center at Lewis Field, Cleveland, Ohio 44135

An approach is described that attempts to bridge the gap between the traditional Reynolds-averaged Navier–Stokes (RANS) simulation and the traditional large-eddy simulation (LES). This approach affords an intermediate resolution of turbulence scales relative to those of RANS and LES and has the characteristics of the very large-eddy simulation (VLES). The very large scales of turbulence are directly calculated, and the effects of the unresolved scales are accounted for by an eddy viscosity model that is evolved from state-of-the-art models used in the RANS approach. The dependent variables and governing equations are based on a temporal filtering with a constant filter width. The contents of both resolved and unresolved scales are regulated by the width of the filter. The dependent variables and governing equations will naturally evolve from RANS to VLES and further toward LES, when the width of the temporal filter is decreased from the turbulent integral timescale to its fraction and all of the way toward the Taylor microtimescale. The subscale model uses a resolution control parameter, which is a function of the temporal filter width, to regulate the content of resolved/unresolved scales. This approach is called the partially resolved numerical simulation. Its mathematical formulation is described. Also, a guideline is provided for selecting the resolution control parameter and the grid spacing that optimizes the accuracy of the numerical simulation. Results from validation studies are then reported.

I. Introduction

MANY engineering applications involve transient flows in which coherent structures play a very important role in determining the turbulent mixing and other turbulence dynamics. It is known that the Reynolds-averaged Navier–Stokes (RANS) simulation cannot capture important turbulent unsteady effects. On the other hand, the large eddy simulation (LES), which typically resolves turbulence scales down to the range of the inertial scales, can be too costly when the resolution of only the relatively larger scales is required. There is a need for approaches that are capable of extracting some of the large-scale unsteady features of turbulent flows at reasonable computational costs, as evidenced by the recent development of various hybrid RANS/LES approaches.[1–9] The basic strategy is to reduce the turbulent eddy viscosity in the fine-grid regions to promote a LES type of behavior and revert to a RANS type of behavior in the coarse grid regions. The switch between RANS and LES is usually based on a criterion in terms of local grid spacing and local flow quantities. Most of the approaches invoke spatially filtered equations for the resolved scales of turbulence, and the constitutive equation of the subgrid model explicitly has the local computational mesh size as a parameter because the local grid spacing is also construed as the local width of the spatial filter. There are several issues associated with the spatially filtered equations and the use of computational mesh size as a parameter in the constitutive equation of subgrid model. The first issue is the commutation error due to the nonuniform computational mesh.[10] The second one is the inconsistency between the filter functions and subgrid models.[11] This inconsistency may give rise to difficulties when simultaneously executing the filter function and subgrid model. For example, the dynamic procedure based on the Germano identity (see Ref. 12) may lead to an unphysical model coefficient. The third issue is that a grid-independent solution cannot be attained. If we accept the premise that small-scale motions tend to have small timescales and use temporal filtering with a fixed filter width to define the large scales of turbulence, together with a subscale model that does not have grid spacing as a parameter in its constitutive equation, then all of these issues can be largely avoided.

In numerical simulation of turbulent flows, there are three kinds of resolutions involved. The first one is the low end of the resolved scales of turbulence, denoted by η_r, which is mainly determined by the modeled subscale eddy viscosity ν_T and can be estimated as $(\nu_T^3/\varepsilon)^{1/4}$ using a simple dimensional analysis. Here, ε is the dissipation rate. The second one is the numerical grid spacing Δ, which must be smaller than η_r to capture numerically the low end of the resolved scales. The third one has its origin in the numerical scheme and is characterized by a numerical viscosity ν_{error}, which will determine a contamination length scale $\eta_{\text{error}} = (\nu_{\text{error}}^3/\varepsilon)^{1/4}$ that must be negligibly small when compared with η_r, that is, $\nu_T \gg \nu_{\text{error}}$. In practice, we require that

$$\Delta \leq \eta_r, \qquad \eta_{\text{error}} \ll \eta_r \tag{1}$$

When subgrid models such as $\nu_T = C_s S \Delta^2$ are used in conjunction with numerical schemes of lower accuracy, for example, the truncation error is of second order, that is, $\sim\Delta^2$, the condition $\nu_T \approx \nu_{\text{error}}$ could occur in some regions and thus, the eddy viscosity of unresolved turbulence would be severely contaminated by the numerical dissipation. In this case, a reduction in contamination is not achieved by just reducing the grid spacing. However, if the constitutive equation of the subgrid model does not use the grid spacing as one of its parameters, and resolves very large eddies with more sophisticated formulations, then condition (1) can be satisfied with relative ease.

In the following sections, we describe the mathematical formulation for the current approach and provide a guideline for selecting the resolution control parameter and the grid spacing that optimizes the accuracy of the numerical simulation. Results from validation studies are then reported.

II. Partially Resolved Numerical Simulation

This approach is based on the premise that small-scale motions tend to have small timescales and a temporal filter with a fixed width is used to define the large-scale turbulence. In partially resolved numerical simulation (PRNS), the governing equations for the resolved part of the turbulent motion are modified Navier–Stokes equations, in which the dependent variables can evolve from the statistical means (as in RANS) to the partially resolved large-scale variables (as in LES), depending on the value of the temporal filter width.

Presented as Paper 2004-0160 at the AIAA 42nd Aerospace Sciences Meeting, Reno, NV, 5–8 January 2004; received 7 November 2004; revision received 22 August 2005; accepted for publication 28 August 2005.

*Aerospace Engineer, Combustion Branch. Associate Fellow AIAA.
†Principal Scientist, Institute for Computational Mechanics in Propulsion, Ohio Aerospace Institute.

The corresponding subscale models can also evolve from representing the effect of all turbulent scales (as in RANS) to representing only the effect of those unresolved scales (as in LES). In between, when the level of resolution is somewhat lower than that of the traditional LES, PRNS becomes a very large-eddy simulation VLES (see Ref. 6). Performing temporal filtering with a constant filter width on the Navier–Stokes equations produces no commutation error. In addition, some general statistical relationships between the instantaneous turbulence and the resolved/unresolved turbulence can be established. These exact relationships can be used to compare directly measured turbulent quantities with their calculated counterparts. The unresolved stresses and fluxes are modeled via a k–ε model, in which k is the kinetic energy of unresolved scales defined by the trace of unresolved stresses and ε is its dissipation rate. A set of modeled transport equations will provide k and ε. The subscale model uses a resolution control parameter (RCP), which is a function of the temporal filter width, to regulate the content of resolved/unresolved scales. By varying this resolution control parameter, we can conduct VLES from RANS toward LES. Most recently, a similar effort has been reported by Girimaji and Abdol-Hamid,[13] and their approach is termed as the partially averaged Navier–Stokes (PANS). From the practical application point of view, the major difference between our approach and PANS lies in the choice of the resolution control parameter and the form of the modeled transport equation for the dissipation rate.

A. Definition of Large-Scale Turbulence

When a homogeneous temporal filter $G(t-t')$ is used, a large-scale variable $\bar{\phi}$ and its density-weighted variable $\tilde{\phi}$ can be defined as

$$\bar{\phi}(t, x_i) = \int \phi(t', x_i) G(t-t')\,\mathrm{d}t', \qquad \tilde{\phi} = \frac{\overline{\rho\phi}}{\bar{\rho}} \tag{2}$$

where the integral is over the entire time domain and G satisfies the condition

$$\int G(t-t')\,\mathrm{d}t' = 1$$

For example, the following top hat filter with the width Δ_T satisfies this condition:

$$G(t-t') = \begin{cases} 1/\Delta_T, & \text{if} \quad |t-t'| \le \Delta_T/2 \\ 0, & \text{otherwise} \end{cases} \tag{3}$$

When this filter is used, the left part of Eq. (2) becomes

$$\bar{\phi}(t, x_i) = \frac{1}{\Delta_T}\int_{t-\Delta_T/2}^{t+\Delta_T/2} \phi(t', x_i)\,\mathrm{d}t' \tag{4}$$

Equation (4) indicates that $\bar{\phi}$ and $\tilde{\phi}$ will become a Reynolds-averaged quantity and a Favre-averaged quantity, respectively, as $\Delta_T \to \infty$. On the other hand, they may become an instantaneous turbulent quantity as $\Delta_T \to 0$. For a finite Δ_T, they represent a quantity determined mainly by the large scales of turbulence. Apparently, Δ_T regulates the content of both resolved and unresolved scales.

B. Governing Equations

Performing operation (2) on the Navier–Stokes equations, we obtain a set of governing equations for the resolved large-scale turbulence as follows:

$$(\bar{\rho}\tilde{u}_i)_{,t} + (\bar{\rho}\tilde{u}_i\tilde{u}_j)_{,j} = -\bar{p}_{,i} - \tau_{ij,j} + \left(2\bar{\mu}\tilde{S}_{ij} - \tfrac{2}{3}\delta_{ij}\bar{\mu}\tilde{S}_{kk}\right)_{,j} \tag{5}$$

$$(\bar{\rho}\tilde{e})_{,t} + (\bar{\rho}\tilde{u}_i\tilde{e})_{,i} = (\bar{\kappa}\tilde{T}_{,i})_{,i} + \overline{pS_{kk}} - q_{i,i} + \left(2\bar{\mu}\widetilde{S_{ij}S_{ij}} - \tfrac{2}{3}\bar{\mu}\widetilde{S_{kk}S_{ii}}\right) + \bar{Q} \tag{6}$$

$$\bar{\rho}_{,t} + (\bar{\rho}\tilde{u}_i)_{,i} = 0, \qquad \bar{p} = \bar{\rho}R\tilde{T} \tag{7}$$

where $S_{ij} = (u_{i,j} + u_{j,i})/2$. In Eqs. (5–7), the subscripts , t and , i represent the temporal and spatial derivatives, respectively; ρ, u_i, T, p, e, and Q are the density, velocity, temperature, pressure, internal energy per unit mass, and radiation rate; μ and κ are the viscosity and heat conductivity; R is the universal gas constant; and τ_{ij} and q_i are the unresolved stresses and heat fluxes,

$$\tau_{ij} \equiv \bar{\rho}(\widetilde{u_iu_j} - \tilde{u}_i\tilde{u}_j), \qquad q_i \equiv \bar{\rho}(\widetilde{u_ie} - \tilde{u}_i\tilde{e}) \tag{8}$$

Note that two types of resolved large-scale variables appear in the preceding equations, $\bar{\phi}$ and $\tilde{\phi}$, where $\bar{\phi}$ is defined by a temporal filtering and $\tilde{\phi}$ is defined by a density-weighted temporal filtering.

C. Time-Averaging Relationships

A few useful relationships between the time average (Reynolds and Favre) of a turbulent variable and the resolved/unresolved quantities will be derived. These relationships will allow us to make a direct comparison between experimentally measured data and results from numerical simulations.

1. *First-, Second-, and Higher-Order Moments*

The definition of Reynolds averaging and Favre averaging of a turbulent variable ϕ can be written as

$$\langle\phi\rangle = \lim_{T\to\infty}\frac{1}{T}\int_{-T/2}^{T/2}\phi\,\mathrm{d}t, \qquad [\phi] = \lim_{T\to\infty}\frac{1}{\langle\rho\rangle T}\int_{-T/2}^{T/2}\rho\phi\,\mathrm{d}t \tag{9}$$

where ϕ can be u_i or u_iu_j, or $u_iu_ju_k$, etc.; T is the entire time domain; $\langle\phi\rangle$ is the pure time-averaged (Reynolds-averaging) quantity; and $[\phi]$ is the density-weighted time-averaged (Favre averaging) quantity.

If we divide T into M intervals, and each interval has a finite width Δ_T, then the Favre-average $[\phi]$ in Eq. (9) can be written as

$$[\phi] = \lim_{T\to\infty}\frac{\Delta_T}{\langle\rho\rangle T}\left(\frac{1}{\Delta_T}\int_{t_1-\Delta_T/2}^{t_1+\Delta_T/2}\rho\phi\,\mathrm{d}t + \cdots + \frac{1}{\Delta_T}\int_{t_i-\Delta_T/2}^{t_i+\Delta_T/2}\rho\phi\,\mathrm{d}t + \cdots + \frac{1}{\Delta_T}\int_{t_M-\Delta_T/2}^{t_M+\Delta_T/2}\rho\phi\,\mathrm{d}t\right) \tag{10}$$

where $M = T/\Delta_T$. Because each component in Eq. (10) represents a top hat temporal filtering that defines a quantity characterizing the resolved large-scale turbulence $(\bar{\rho}\tilde{\phi})^{(i)}$, Eq. (10) can be written as

$$[\phi] = \lim_{M\to\infty}\frac{1}{\langle\rho\rangle M}\sum_{i=1}^{M}(\bar{\rho}\tilde{\phi})^{(i)} \tag{11}$$

The right-hand side is an ensemble averaging, and we denote it by $\{\bar{\rho}\tilde{\phi}\}$. We also notice that $\langle\rho\rangle \equiv \{\bar{\rho}\}$; therefore, Eq. (11) becomes $[\phi] = \{\bar{\rho}\tilde{\phi}\}/\{\bar{\rho}\}$. Consequently, we may establish the following relationships:

$$[u_i] = U_i = \{\bar{\rho}\tilde{u}_i\}/\{\bar{\rho}\}, \qquad [u_iu_j] = \{\bar{\rho}\widetilde{u_iu_j}\}/\{\bar{\rho}\}$$
$$[u_iu_ju_k] = \{\bar{\rho}\widetilde{u_iu_ju_k}\}/\{\bar{\rho}\}, \ldots \tag{12}$$

2. *Reynolds Stresses R_{ij} and Resolved Large-Scale Stresses T_{ij}*

According to the conventional definition, we may write the Reynolds stresses R_{ij} as

$$R_{ij} = \langle\rho(u_i - [u_i])(u_j - [u_j])\rangle/\langle\rho\rangle = [u_iu_j] - [u_i][u_j] \tag{13}$$

Using the definition of the unresolved stresses τ_{ij}, we may write $\{\tau_{ij}\} = \{\bar{\rho}\widetilde{u_iu_j}\} - \{\bar{\rho}\tilde{u}_i\tilde{u}_j\}$. From Eqs. (12) and (13), we obtain

$$R_{ij} = \{\tau_{ij}\}/\{\bar{\rho}\} + \{\bar{\rho}\tilde{u}_i\tilde{u}_j\}/\{\bar{\rho}\} - \{\bar{\rho}\tilde{u}_i\}\{\bar{\rho}\tilde{u}_j\}/\{\bar{\rho}\}\{\bar{\rho}\} \tag{14}$$

If we define the resolved large-scale stresses T_{ij} as

$$T_{ij} \equiv \{\bar{\rho}(\tilde{u}_i - \{\bar{\rho}\tilde{u}_i\}/\{\bar{\rho}\})(\tilde{u}_j - \{\bar{\rho}\tilde{u}_j\}/\{\bar{\rho}\})\}/\{\bar{\rho}\}$$
$$= \{\bar{\rho}\tilde{u}_i\tilde{u}_j\}/\{\bar{\rho}\} - \{\bar{\rho}\tilde{u}_i\}\{\bar{\rho}\tilde{u}_j\}/\{\bar{\rho}\}\{\bar{\rho}\} \tag{15}$$

Equation (14) then becomes

$$R_{ij} = T_{ij} + \{\tau_{ij}\}/\{\bar{\rho}\} \tag{16}$$

Equation (14) or (16) will allow us to calculate exactly the Reynolds stresses using the solution of the resolved field in conjunction with the modeled unresolved stresses, for example, Eq. (19), and to make apple-to-apple comparisons with experimental data. A similar relationship can be derived for the scalar fluxes:

$$R_i = T_i + \{q_i\}/\{\bar{\rho}\} \tag{17}$$

where $R_i = \langle \rho(u_i - [u_i])(e - [e])\rangle/\langle\rho\rangle$, $T_i = \{\bar{\rho}\tilde{u}_i\tilde{e}\}/\{\bar{\rho}\} - \{\bar{\rho}\tilde{u}_i\}\{\bar{\rho}\tilde{e}\}/\{\bar{\rho}\}\{\bar{\rho}\}$, and q_i is the unresolved flux defined in Eq. (8) and modeled by Eq. (19). In this section, several averaging procedures are employed. Reynolds averaging is a pure time averaging denoted by $\langle\phi\rangle$ (usually for incompressible flows). Farve averaging is a density-weighted time averaging denoted by $[\phi]$ (usually for compressible flows). The ensemble averaging is denoted by $\{\phi\}$. It can be shown that an ensemble averaging is equivalent to a pure time averaging, that is, $\{\phi\} = \langle\phi\rangle$, if the turbulence is statistically steady.

D. Modeling of Unresolved Turbulent Stresses and Fluxes

1. *Nonlinear Stress and Flux Model*

The exact transport equation for the unresolved stresses τ_{ij} can be derived according to its definition, $\bar{\rho}(\widetilde{u_i u_j} - \tilde{u}_i\tilde{u}_j)$. The equation has the following form:

$$\tau_{ij,t} + (\tilde{u}_k\tau_{ij})_{,k} = D_{ij} + \Phi_{ij} + P_{ij} - \bar{\rho}\varepsilon_{ij} \tag{18}$$

where

$$\begin{aligned} D_{ij} = &-(\bar{\rho}\widetilde{u_i u_j u_k} - \bar{\rho}\widetilde{u_i u_j}\tilde{u}_k) + \left\{2\bar{\mu}\widetilde{u_j S_{ik}} - \tfrac{2}{3}\delta_{ik}\bar{\mu}\widetilde{u_j S_{mm}}\right. \\ &\left. - \left[\widetilde{u_j}\left(2\bar{\mu}\tilde{S}_{ik} - \tfrac{2}{3}\delta_{ik}\bar{\mu}\tilde{S}_{mm}\right)\right]\right\}_{,k} + (\tau_{ik}\tilde{u}_j + \tau_{jk}\tilde{u}_i)_{,k} \\ &- (\overline{pu_j}\delta_{ik} + \overline{pu_i}\delta_{jk} - \bar{p}\tilde{u}_j\delta_{ik} - \bar{p}\tilde{u}_i\delta_{jk})_{,k} \\ &+ \left\{2\bar{\mu}\widetilde{u_i S_{jk}} - \tfrac{2}{3}\delta_{jk}\bar{\mu}\widetilde{u_i S_{mm}} - \left[\tilde{u}_i\left(2\bar{\mu}\tilde{S}_{jk} - \tfrac{2}{3}\delta_{jk}\bar{\mu}\tilde{S}_{mm}\right)\right]\right\}_{,k} \end{aligned}$$

$$\Phi_{ij} = 2\overline{pS_{ij}} - 2\bar{p}\tilde{S}_{ij}$$

$$P_{ij} = -\tau_{ik}\tilde{u}_{j,k} - \tau_{jk}\tilde{u}_{i,k}$$

$$\begin{aligned} \bar{\rho}\varepsilon_{ij} = &\left[2\bar{\mu}(\widetilde{S_{ik}u_{j,k}} + \widetilde{S_{jk}u_{i,k}}) - \tfrac{4}{3}\bar{\mu}\widetilde{S_{mm}S_{ij}}\right] \\ &- \left[2\bar{\mu}(\tilde{S}_{ik}\tilde{u}_{j,k} + \tilde{S}_{jk}\tilde{u}_{i,k}) - \tfrac{4}{3}\bar{\mu}\tilde{S}_{mm}\tilde{S}_{ij}\right] \end{aligned}$$

In principle, Eq. (18) could be used in the numerical simulation; however, for simplicity and practical applications, we will consider only the following algebraic models for the unresolved stresses and fluxes, with Eq. (18) being traced to provide a transport equation for the unresolved turbulent kinetic energy:

$$\tau_{ij} = -2\mu_T\left(\tilde{S}_{ij} - \tfrac{1}{3}\delta_{ij}\tilde{S}_{kk}\right) + \tfrac{1}{3}\delta_{ij}\tau_{kk} + \cdots, \qquad q_i = -\kappa_T\tilde{T}_{,i} \tag{19}$$

where the ellipses are the nonlinear terms representing the effects of anisotropy and swirling,[14] which may become important when the unresolved scales become sufficiently large, μ_T is the subscale eddy viscosity contributed by the unresolved scales, and κ_T are the eddy diffusivities for the heat, which are often modeled as $\kappa_T = \mu_T/Pr_T$, where Pr_T is the turbulent Prandtl number.

2. *Eddy Viscosity Model for Unresolved Scales of Turbulence*

We consider the following factors that could affect μ_T: the unresolved turbulent kinetic energy k and its dissipation rate ε, a global turbulent time integral scale T for a given turbulent flow, and the temporal filter width Δ_T, which is a fraction of T. Then, $\mu_T/\bar{\rho} = f(k, \varepsilon, \Delta_T, T)$. When the π theory of dimensional analysis is applied, it leads to $\mu_T/(\bar{\rho}k^2/\varepsilon) = f(\Delta_T/T)$. The right-hand side can be expanded as $f = C_0 + C_1(\Delta_T/T) + C_2(\Delta_T/T)^2 + \cdots$, where C_0 must be zero because the subscale eddy viscosity approaches zero as $\Delta_T \to 0$. If we take the leading term as a first-order approximation, we have

$$\mu_T = (\Delta_T/T)C_1\bar{\rho}(k^2/\varepsilon) \tag{20}$$

Now, the subscale eddy viscosity is directly proportional to the ratio of Δ_T/T, even if, strictly speaking, it is mathematically valid only for small Δ_T/T. For practical application, when this ratio goes to one, the subscale eddy viscosity should approach its RANS counterpart. Therefore, we choose C_1 to be the familiar C_μ used in the RANS model, which is given by, for example, the sophisticated model formula[15,16] or a value of 0.09 as in the standard k–ε model. From the preceding discussion, we propose the following model for the subscale eddy viscosity:

$$\mu_T = \mathrm{RCP}\cdot C_\mu\cdot\bar{\rho}\cdot k^2/\varepsilon, \qquad \mathrm{RCP} = \Delta_T/T \tag{21}$$

where RCP explicitly regulates the subscale eddy viscosity. Equation (21) is a simple model for explicitly taking into account the effect of the parameter Δ_T/T on the resolved flowfield. More sophisticated formulations are possible, for example,

$$\mathrm{RCP} = [1 - \exp(-A_1\cdot\Delta_T/T)]^{A_2} \tag{22}$$

where A_1 and A_2 are constants and need to be determined.

3. *k–ε Transport Equation Models*

The variables k and ε will be determined by their modeled transport equations. We start from Eq. (18): If the diffusion term D_{ij} is modeled by an eddy viscosity diffusion, and the term P_{ij} is modeled via Eq. (19), then the trace of Eq. (18), $k = \tau_{ii}/2\bar{\rho}$, becomes

$$\frac{\partial}{\partial t}\bar{\rho}k + \frac{\partial}{\partial x_i}\bar{\rho}\tilde{u}_i k = \frac{\partial}{\partial x_i}\left[(\bar{\mu} + \mu_T)\frac{\partial}{\partial x_i}k\right] + 2\mu_T\tilde{S}_{ij}\tilde{S}_{ij} - \bar{\rho}\varepsilon \tag{23}$$

where the dissipation rate is defined by $\bar{\rho}\varepsilon_{ii}/2$, that is,

$$\bar{\rho}\varepsilon = \left(2\bar{\mu}\widetilde{S_{ij}S_{ij}} - \tfrac{2}{3}\bar{\mu}\widetilde{S_{mm}S_{ii}}\right) - \left(2\bar{\mu}\tilde{S}_{ij}\tilde{S}_{ij} - \tfrac{2}{3}\bar{\mu}\widetilde{S_{mm}}\widetilde{S_{ii}}\right) \tag{24}$$

The exact transport equation for the dissipation rate can be derived but is very complicated. A model equation can alternatively be constructed by analogy to Eq. (23) as

$$\begin{aligned} \frac{\partial}{\partial t}\bar{\rho}\varepsilon + \frac{\partial}{\partial x_i}\bar{\rho}\tilde{u}_i\varepsilon = &\frac{\partial}{\partial x_i}\left[(\bar{\mu} + \mu_T)\frac{\partial}{\partial x_i}\varepsilon\right] \\ &+ C_{\varepsilon 1}2\mu_T\tilde{S}_{ij}\tilde{S}_{ij}\frac{\varepsilon}{k} - C_{\varepsilon 2}\frac{\bar{\rho}\varepsilon^2}{k} \end{aligned} \tag{25}$$

where $C_{\varepsilon 1}$ and $C_{\varepsilon 2}$ are the model coefficients. From the theory of energy cascade from large scales to small scales,[17] the dissipation rate of turbulent energy is mainly determined by the rate of energy cascade: In PRNS, we mainly are interested in the very large scales of motion; hence, it is reasonable to expect that the modeled dissipation equation for the unresolved turbulence has a similar form to the one in the RANS model and the model coefficients will have about the same values as their RANS counterparts. Therefore, we adopt the common values of $C_{\varepsilon 1} = 1.45$ and $C_{\varepsilon 2} = 1.92$. Of course, they can be further constructed as the functions of local turbulence quantities.[18]

4. *Resolution Control Parameter*

The RCP is used to regulate the scale content of the resolved field via the subscale eddy viscosity model for unresolved scales. More specifically, it implicitly and nonlinearly determines the low-end of the resolved large scales. When RCP = 1, the low end of the resolved scales is the integral length scale of the turbulence, therefore, the unresolved field contains all scales of the turbulence, and this is a RANS simulation. As the value of RCP decreases, the low end of the resolved scales is expected to move toward smaller scales, and the unresolved field now contains fewer large scales. Because most of the vorticity is associated with small-scale motions, and most of

the energy is associated with large-scale motions, the vorticity of the resolved field should increase and the turbulent kinetic energy of the unresolved field should decrease. In addition, the subscale eddy viscosity should also become smaller to reflect the reduced effects of a down sized unresolved field. It will be demonstrated in the next section that, for the cases considered, the reduction in RCP does yield the physically consistent behavior already described.

In planning a VLES for a given turbulent flow, one may often ask the following questions: How do we choose the value of RCP from the outset? How do we estimate the corresponding numerical grid size needed for this simulation? For a given numerical grid size, how do we choose RCP to yield a resolved scale level that the numerical grid can capture? To answer these questions, let us first introduce a useful length scale by invoking a Kolmogorov type of analysis. This length scale, η_{PRNS}, is the effective size of the dissipative eddies permitted by the subscale eddy viscosity ν_T and the dissipation rate ε of the unresolved field and is estimated by

$$\eta_{\text{PRNS}} = \left(\nu_T^3/\varepsilon\right)^{\frac{1}{4}} \tag{26}$$

Naturally, η_{PRNS} should be the low end of the resolved scales in PRNS. Because Eq. (21) can be formally written as $\nu_T = \text{RCP} \cdot \nu_{\text{RANS}} \cdot (k^2/\varepsilon)/(k_{\text{RANS}}^2/\varepsilon_{\text{RANS}}) \le \text{RCP} \cdot \nu_{\text{RANS}}$, then Eq. (26) leads to

$$\eta_{\text{PRNS}} \le \text{RCP}^{\frac{3}{4}} \cdot \left(\nu_{\text{RANS}}^3/\varepsilon\right)^{\frac{1}{4}} \approx \text{RCP}^{\frac{3}{4}} \cdot \left(\nu_{\text{RANS}}^3/\varepsilon_{\text{RANS}}\right)^{\frac{1}{4}}$$

$$= \text{RCP}^{\frac{3}{4}} \cdot \eta_{\text{RANS}} \tag{27}$$

where $\eta_{\text{RANS}} = (\nu_{\text{RANS}}^3/\varepsilon_{\text{RANS}})^{\frac{1}{4}}$ represents a scale due to the RANS model eddy viscosity and the dissipation rate, which is of the order of the turbulent integral length scale ℓ. On the other hand, the numerical grid size Δ should be smaller or equal to η_{PRNS}. Therefore,

$$\text{RCP} \ge (\Delta/\ell)^{\frac{4}{3}} \tag{28}$$

Equation (28) is useful in several ways. When RCP is given from the outset, it can be used to estimate the largest possible value of the grid spacing relative to the turbulent integral length scale. Alternatively, when the grid spacing is given from the outset, Eq. (28) can be used to estimate the smallest possible value of RCP that the given grid size can support.

We will first discuss the case of specifying RCP from the outset of a simulation. Note here that all of the simulations presented in the next section belong to this case. Based on the available information on the flow and geometry, we may estimate the global integral timescale T and the integral length scale ℓ. For a VLES, we may choose the width of the temporal filter Δ_T as a fraction of T, for example, $\Delta_T/T \approx 0.38$, this determines RCP from Eq. (21). Subsequently, an estimate of the compatible grid spacing Δ is obtained via Eq. (28). Furthermore, let L be the length of the computational domain and keep in mind that Δ now is a representative of the low-end scale of the resolved motions; then, the number of grid points needed for the PRNS simulation, $N_{\text{PRNS}} \approx (L/\Delta)^3$, can be written as

$$N_{\text{PRNS}} = (L/\ell)^3 \cdot (\ell/\Delta)^3 = N_{\text{RANS}} \cdot \text{RCP}^{-\frac{9}{4}} \tag{29}$$

where $N_{\text{RANS}} \equiv (L/\ell)^3$ is the estimation of the grid points for the RANS calculation. Based on the number of grid points needed for a RANS calculation and the chosen value of RCP, Eq. (29) provides an estimation of the number of grid points needed for a PRNS simulation.

In the case of having to work with a given number of grid points and/or a given grid size distribution, we may judiciously choose a region in the flowfield and use the characteristic grid size Δ and an estimated integral length scale ℓ in this region to estimate the value of RCP via Eq. (28). A much more sophisticated way is to first carry out the RANS calculation to obtain the field of local ℓ, then together with the given local grid spacing, a field of local RCP is estimated via Eq. (28). Subsequently, this field of local RCP is used in the PRNS calculation. Note that the analysis in Sec. II.D.2

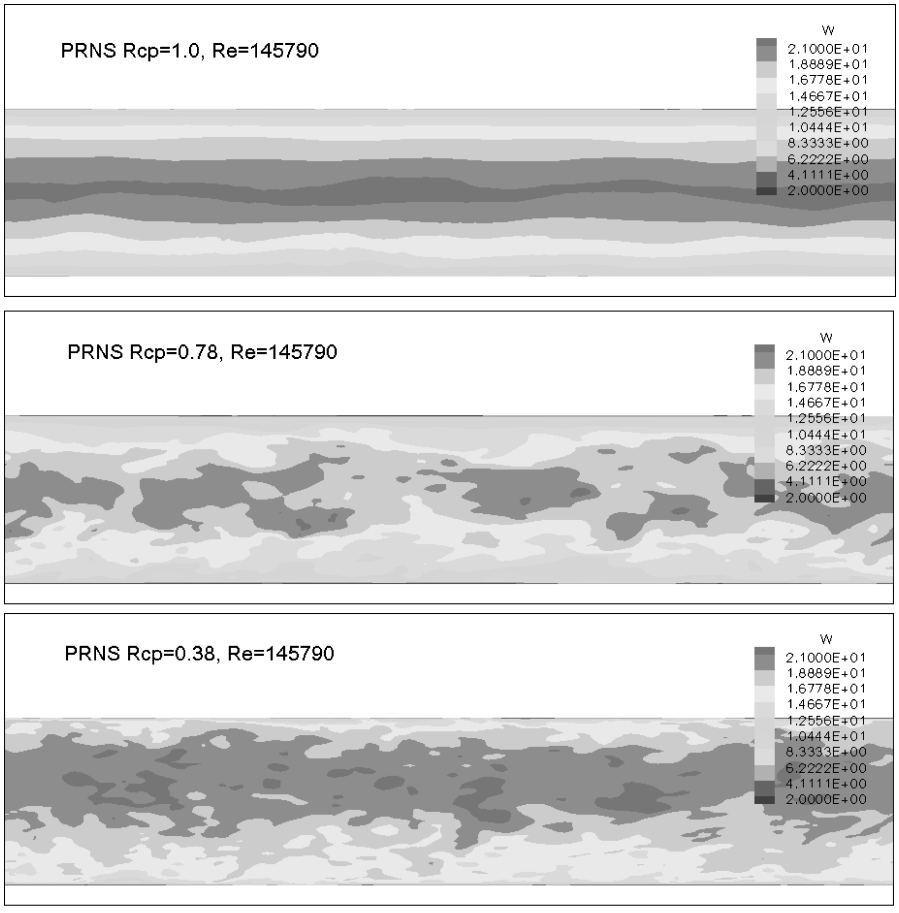

Fig. 1 Contours of axial velocity using different RCPs; simulations evolve from RANS toward LES.

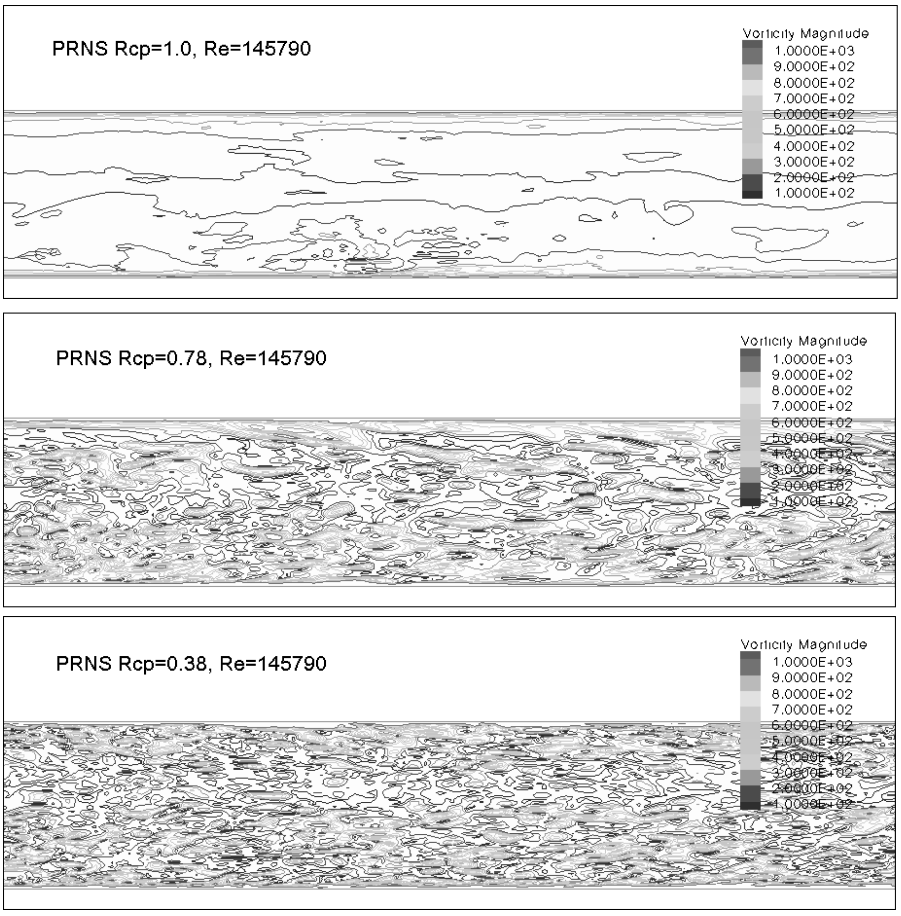

Fig. 2 Contours of vorticity magnitude with different RCPs.

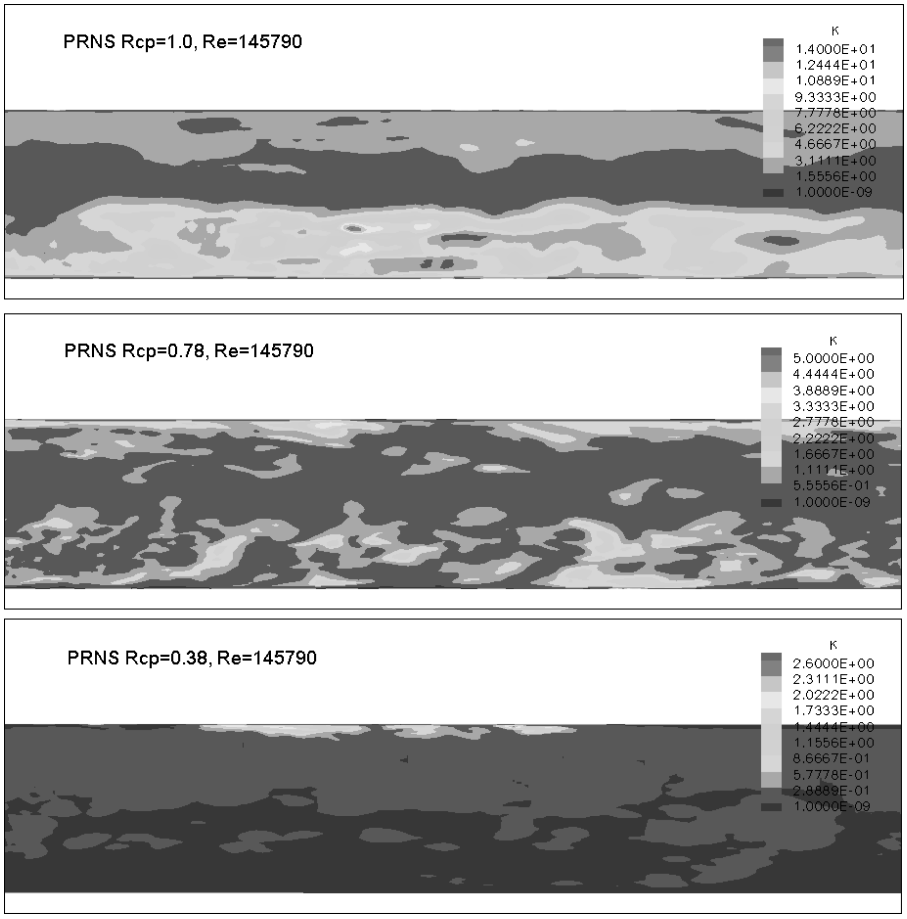

Fig. 3 Contours of kinetic energy of unresolved scales with different RCPs.

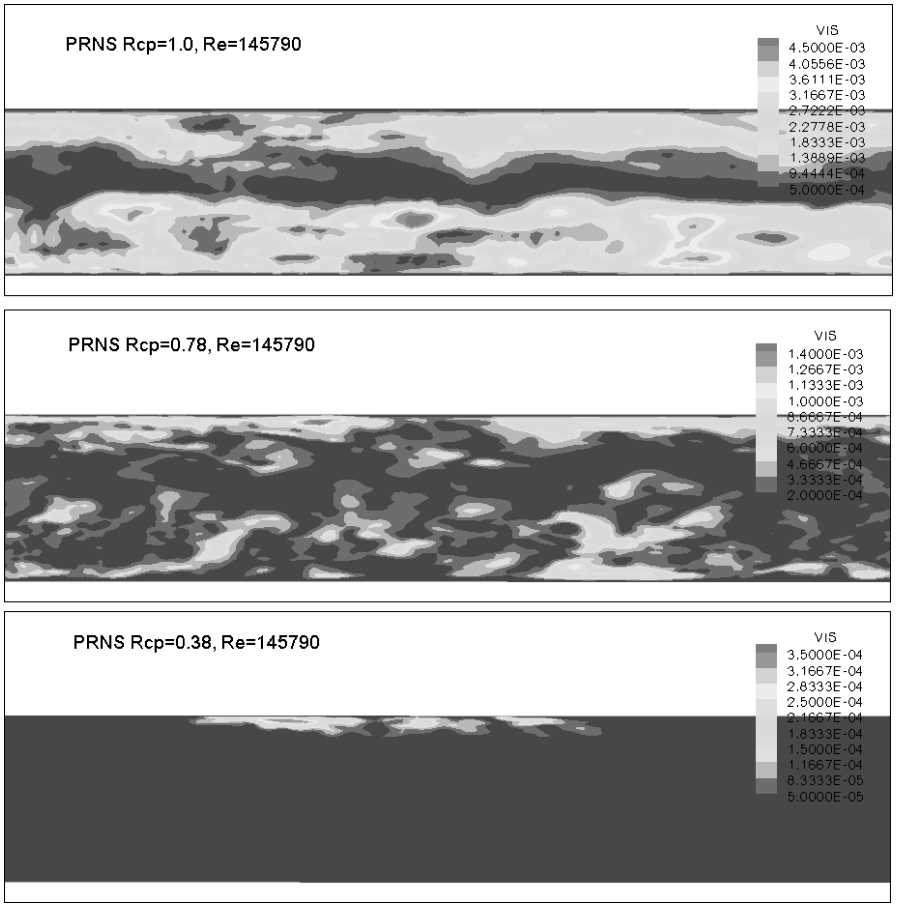

Fig. 4 Contours of effective eddy viscosity with different RCPs.

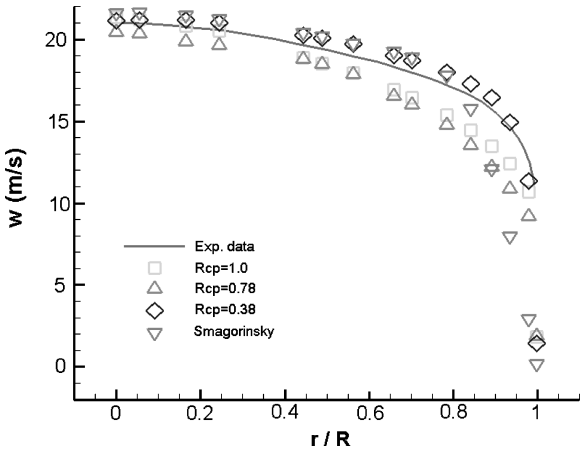

Fig. 5 Time-averaged axial velocities with different RCPs compared with experimental data; $Re = 1.4579 \times 10^5$.

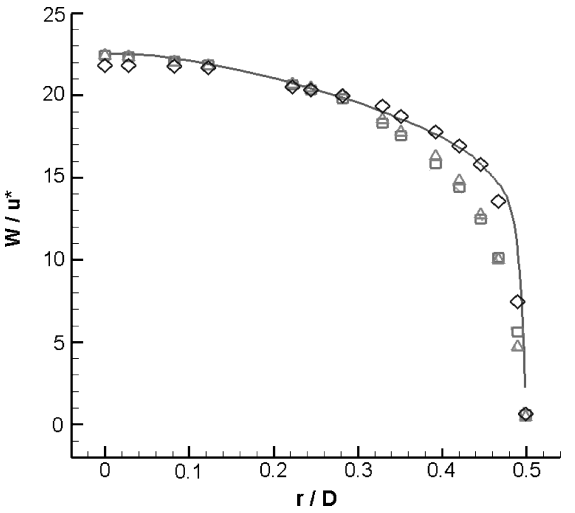

Fig. 6 Comparison of axial mean velocity with experimental data at Reynolds number 1.5×10^4: ——, experimental data; □, RCP = 1.0; △, RCP = 0.78; and ◇, RCP = 0.38.

still holds when the global integral timescale T is replaced with the local integral timescale. We will examine this elaborate way of estimating the RCP field in our future work.

III. Validation: Simulation of Fully Developed Turbulent Pipe Flows

The numerical platform is a NASA in-house code for simulating turbulent combustion in propulsion systems. A detailed description of this code may be found in two reports.[19,20] It employs a cell-centered finite volume method on unstructured grids, and it uses a dual-time-stepping procedure for time-accurate simulations. The numerical accuracy of this code is formally second order. It already has a two-equation k–ε algebraic nonlinear model for the Reynolds stress. In the context of PRNS, the mathematical form of the governing equations to be solved are identical to those already implemented in the code except that the turbulent stresses and fluxes are to be regulated by an RCP. Therefore, this existing code is already in a position to perform PRNS.

The AGARD advisory report provides the experimental data[21] of fully developed turbulent pipe flows. The test case PCH04/re15e4 is for a relatively high Reynolds number, 1.4579×10^5, based on the diameter and maximum velocity. Only the mean flow data are available for comparison. The test case PCH03 is for a lower Reynolds number, $Re_\tau = 1382$ (based on the frictional velocity), and both the axial mean velocity and its rms value are available.

We have performed PRNS calculations for three different Reynolds numbers: $Re = 7 \times 10^3$, 1.5×10^4, and 1.4579×10^5. Variation of Reynolds number is accomplished through changing the maximum velocity. The pipe diameter and the length of the computational domain are 0.12936 and 0.6468 m, respectively. The periodic boundary condition was applied at the inlet and outlet boundaries. At the wall, a generalized and unified wall function[22] was applied. This wall function is valid for various pressure gradients including those associated with zero skin friction. The initial flowfield was specified with a randomly disturbed profile. The numerical grid consists of about 900,000 hexahedral elements, and this is consistent with an estimation from Eq. (29). For a typical RANS simulation, around 28 grid points are distributed along the diameter. If the same grid spacing is used along the 5-diam-long pipe, then the total number of grid points will be about 100,000. If we choose RCP = 0.38, then Eq. (29) suggests that about 900,000 grid points will be needed for a PRNS simulation. Note that the same grid distribution was used for all of the other simulations using larger values of RCP.

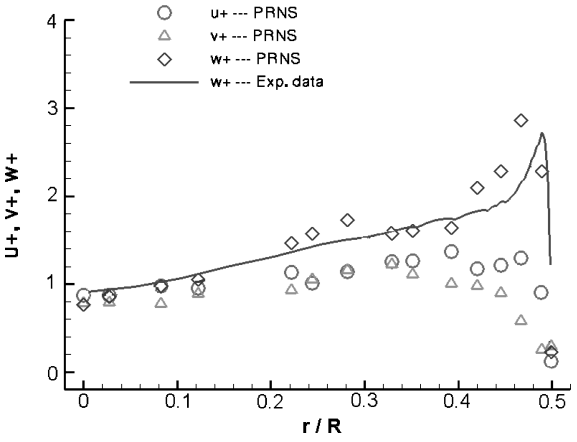

Fig. 7 Comparison of rms fluctuating velocities with experimental data at Reynolds number 1.5×10^4; experimental data have only axial velocity component.

For the pipe flow at a higher Reynolds number $Re = 1.4579 \times 10^5$, Fig. 1 shows the features of the instantaneous contours of axial velocity for three values of RCP: 1.0, 0.78, and 0.38. Figure 1 shows that the resolved scales become finer and finer as RCP becomes smaller and smaller, and the simulated flows display characteristics from that of the RANS type toward that of the LES type. The same phenomena are also clearly shown in Figs. 2–4, which are contours of vorticity magnitude, kinetic energy of unresolved scales, and effective eddy viscosity, respectively. Note that, as RCP decreases, the vorticity magnitude of the resolved field increases, whereas both the kinetic energy and the effective eddy viscosity of the unresolved field decrease. As discussed in the preceding section, this is consistent with the turbulence physics. In Fig. 5, the axial mean velocity profiles obtained from these simulations are compared with the experimental data. The best result is given by RCP = 0.38, for which a larger range of turbulent scales have been resolved.

The results for the pipe flow at Reynolds number of $Re = 1.5 \times 10^4$ are shown in Figs. 6–8. Figure 6 shows a comparison

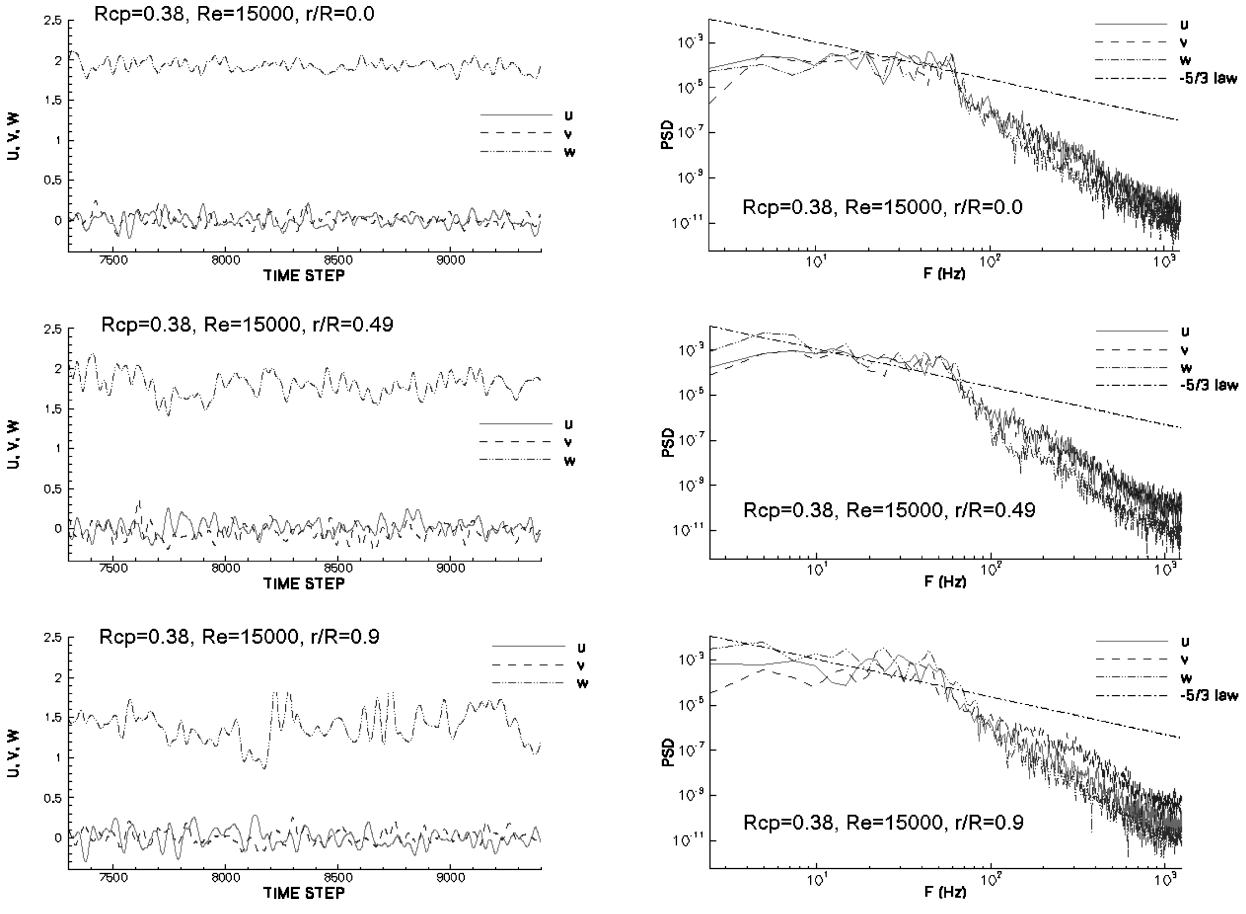

Fig. 8 Velocity signals and respective spectrums at several locations for Reynolds number 1.5×10^4.

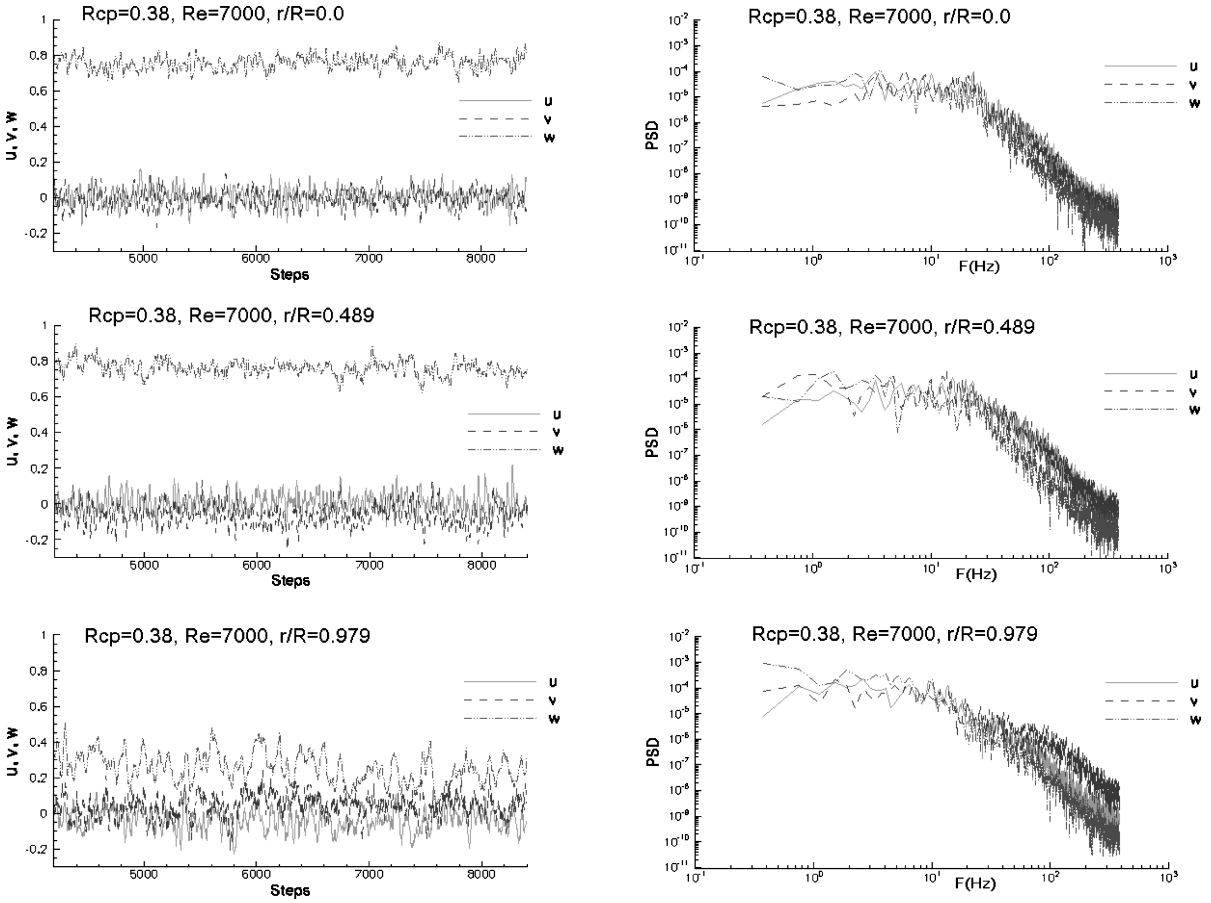

Fig. 9 Velocity signals and respective spectrums at several locations for low-Reynolds-number pipe flow.

of the calculated mean velocity (normalized by the wall friction velocity) with the experimental data.[23] As expected, the simulation with RCP = 0.38 gives the best result because it directly calculates the motions of a larger range of scales. Figure 7 presents the rms values of the fluctuating velocities of the resolved field obtained with RCP = 0.38. The experimental data only have the axial component. It is apparent that the calculated axial rms velocity component is in good agreement with the experimental data. In the simulation, we dispatched 15 probes along the radius from the centerline toward the wall to record the time history of the resolved flowfield. Various statistics of the resolved field have been analyzed, including the power spectrum density of the fluctuating velocities. The velocity signals at three locations, that is, the centerline, the half-way point between the centerline and the wall, and the near wall and their power spectrum density (PSD) for the simulation with RCP = 0.38 are shown in Fig. 8. These broadband power spectrums suggest that a range of large-scale motions have been captured by PRNS.

For the lower Reynolds number, $Re = 7 \times 10^3$, the simulations were carried out for three values of RCP: 1.0, 0.47, and 0.38. The axial mean velocity, its fluctuations, and time power spectrums are all looking reasonable, but unfortunately, there are no experimental data available for this low-Reynolds-number case. Here, we present only Fig. 9 to demonstrate that a broadband power spectrum of the axial velocity was also obtained with RCP = 0.38.

IV. Sample Application: Nonreacting Flow in a Single Injector Flame Tube

The injector used in an industrial combustor is chosen for the current application. The flowfield inside this single injector flame tube is representative of what happens inside the real combustor: massive separation, strong recirculation and swirling, etc. This flow

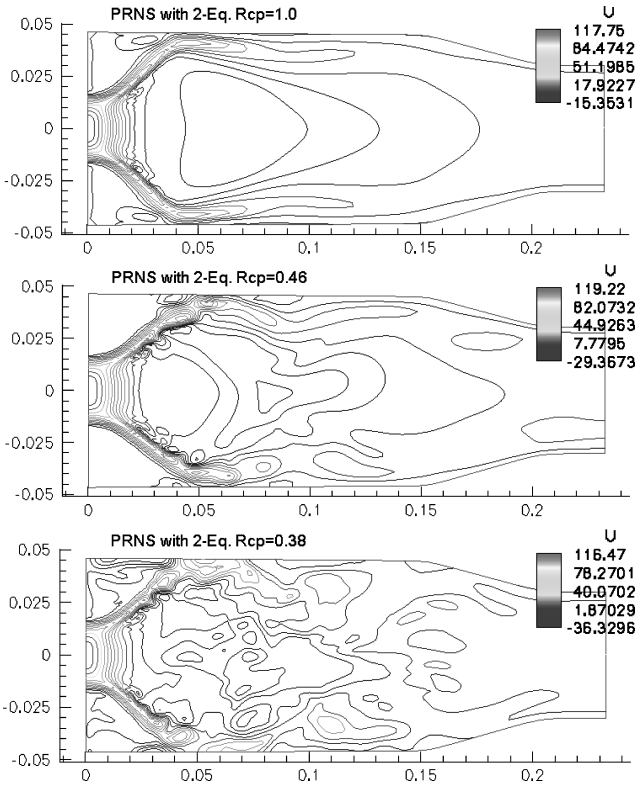

Fig. 10 Contours of axial velocity with different RCPs; simulations move from RANS toward LES.

has been studied both experimentally and numerically (LES[24]). The combustion chamber is a rectangular box. A highly swirling jet is injected from a circular inlet. The Reynolds number based on the inlet axial velocity and diameter is about $Re = 3.2 \times 10^6$. A grid of 495,000 elements was used in the simulation, and this is consistent with the estimation provided by Eq. (29). At the inlet, only the mean profiles of velocities, density, and temperature are specified. At the outlet, simple extrapolation is used to minimize the possible

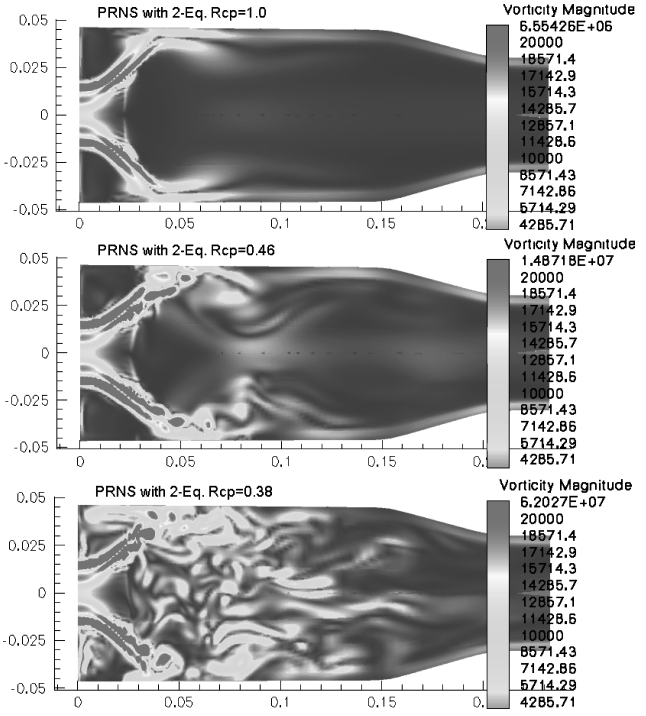

Fig. 11 Contours of vorticity magnitude with different RCPs.

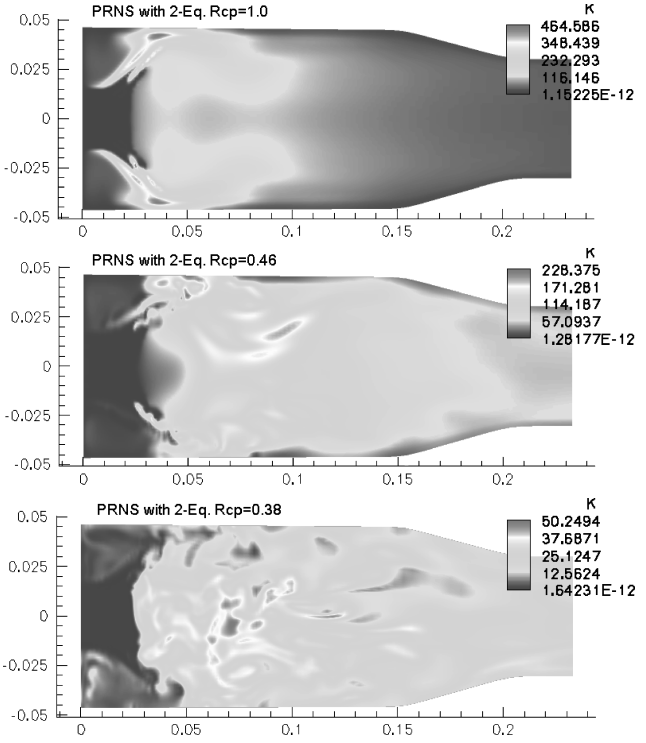

Fig. 12 Contours of kinetic energy of unresolved scales; simulations evolve from RANS toward LES as RCP decreases.

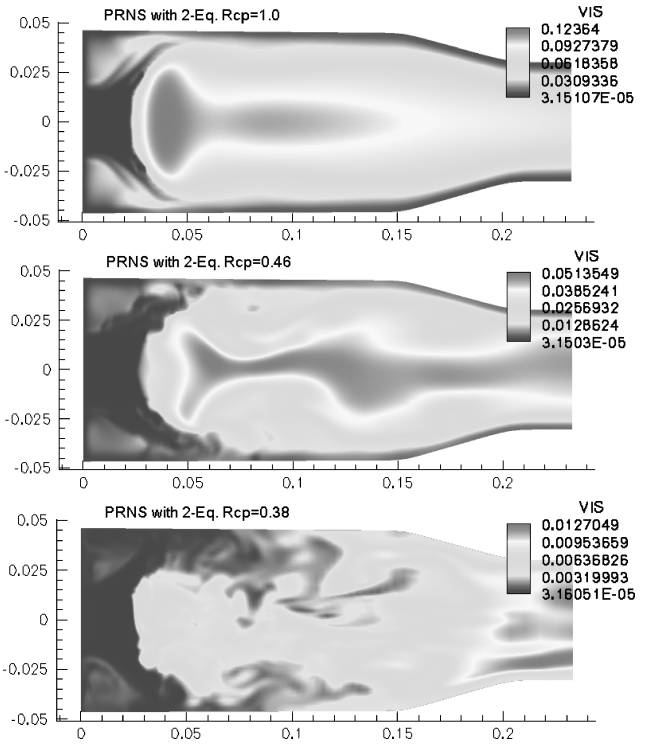

Fig. 13 Contours of effective eddy viscosity with different RCPs.

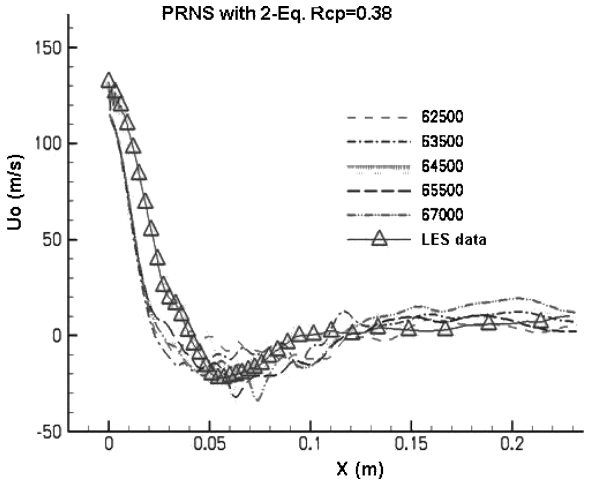

Fig. 14 Instantaneous axial velocities along centerline compared with mean LES data.

unphysical reflections. Figures 10 and 11 show the instantaneous contours of the axial velocity and the vorticity magnitude, respectively. They are obtained from three different values of RCP: 1.0, 0.46, and 0.38. Figures 12 and 13 show the instantaneous features of the kinetic energy of the unresolved scales and the effective eddy viscosity. These results demonstrate again that reducing the resolution control parameter will change the characteristics of simulation from RANS toward LES. Figure 14 shows the comparison between several instantaneous centerline axial velocity distributions with the mean value provided by LES data.[24] Apparently, the simulation with RCP = 0.38 and a relatively coarse grid spacing captured many features of LES. Figure 15 shows the time history of the velocity components and their power spectra at a centerline location inside the recirculation region. The broadband feature of the power spectrum clearly indicates that a wide range of large-scale turbulence has been captured by PRNS.

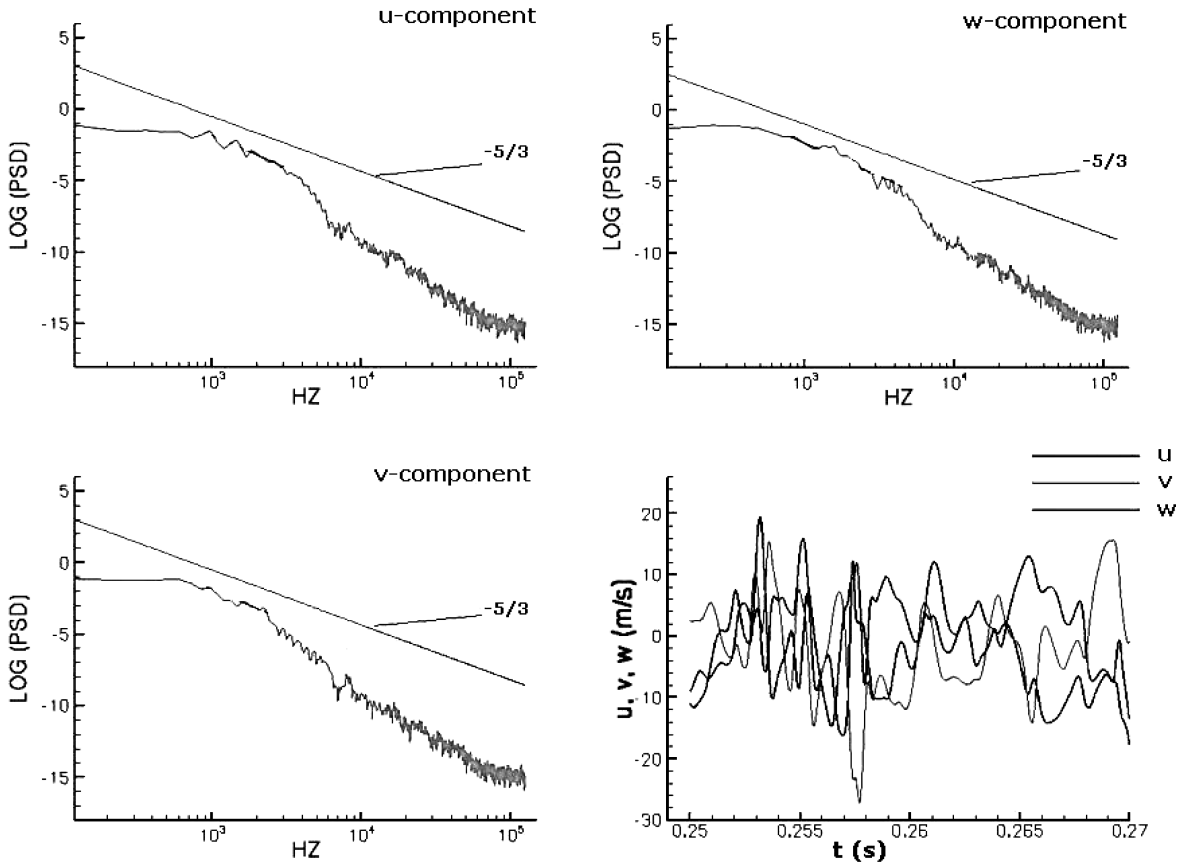

Fig. 15 Fluctuating velocities of resolved field and their time PSD at $x = 0.1$ m, $y = 0$, and $z = 0$.

V. Conclusions

Under the premise that small-scale motions also tend to have small timescales, the large-scale turbulence is defined by a temporal filter with a fixed filter width. This eliminates the problem of commutation errors when the governing equations are being filtered. In addition, exact relationships can be established between various time-averaged quantities (the mean velocity, the Reynolds stresses, etc.) and the statistics calculated from the solution of the resolved field and the models for the unresolved scales. This will allow apple-to-apple comparison between the measured data and the calculated results.

The effects of the unresolved field on the resolved field are accounted for by a subscale eddy viscosity. We have proposed a subscale eddy viscosity model that has a resolution control parameter to regulate implicitly and nonlinearly the low end of the resolved large scales. At the present time, the overall model is intended for the VLES. We choose the low end of the resolved scales to be the size of the dissipative eddies permitted by the effective eddy viscosity and the dissipation rate of the unresolved field, and this enables us to establish guidelines for selecting the resolution control parameter and the numerical grid spacing that optimizes the accuracy of the numerical simulation.

The validation and application of the overall approach, termed here PRNS, have successfully been carried out using a fully developed turbulent pipe flows at different Reynolds numbers and a flow in a single-injector flame tube. These results have demonstrated that this approach is quite promising for conducting a VLES of turbulent flows from RANS toward LES. To continue its validation and to further its improvement, we will apply it to the flow analysis of several fuel injectors recently investigated in test rigs.

Acknowledgments

This work was supported by the NASA Ultra Efficient Engine Technology Project. We thank Jeffrey Moder for his help with the code implementation.

References

[1]Bush, R., and Mani, M., "A Two-Equation Large Eddy Stress Model for High Subgrid Shear," AIAA Paper 2001-2561, June 2001.

[2]Georgiadis, N. J., Iwan, J., Alexander, D., and Reshotko, E., "Development of a Hybrid RANS/LES Method for Compressible Mixing Layer Simulations," AIAA Paper 2001-0289, Jan. 2001.

[3]Fan, T. C., Tian, M., Edwards, J. R., Hassan, H. A., and Baurle, R. A., "Validation of a Hybrid Reynolds-Averaged /Large-Eddy Simulation Method for Simulating Cavity Flameholder Configuration," AIAA Paper 2001-2929, June 2001.

[4]Menter, F. R., Kuntz, M., and Bender, R., "A Scale-Adaptive Simulation Model for Turbulent Flow Predictions," AIAA Paper 2003-0767, Jan. 2003.

[5]Spalart, P. R., "Strategies for Turbulent Modeling and Simulations," *International Journal of Heat and Fluid Flow*, Vol. 21, March 2000, pp. 252–263.

[6]Speziale, C. G., "Turbulence Modeling for Time-Dependent RANS and VLES: A Review," *AIAA Journal*, Vol. 36, No. 2, 1998, pp. 173–184.

[7]Arunajatesan, S., and Sinha, N., "Unified Unsteady RANS–LES Simulations of Cavity Flow Fields," AIAA Paper 2001-0516, Jan. 2001.

[8]Batten, P., Goldberge, U., and Chakravarthy, S., "LNS—An Approach Towards Embedded LES," AIAA Paper 2002-0427, Jan. 2002.

[9]Von Tarzi, D. A., and Fasel, H. F., "A New Flow Simulation Methodology Applied to the Turbulent Backward-Facing Step," AIAA Paper 2002-0429, Jan. 2002.

[10]Ghosal, S., and Moin, P., "The Basic Equations for the Large Eddy Simulation of Turbulent Flows in Complex Geometry," *Journal of Computational Physics*, Vol. 118, April 1995, pp. 24–37.

[11]Clark, R. A., Ferziger, J. H., and Reynolds, W. C., "Evaluation of Subgrid-Scale Models Using an Accurately Simulated Turbulent Flow," *Journal of Fluid Mechanics*, Vol. 91, 1976, pp. 1–16.

[12]Germano, M., Piomelli, U., Moin, P., and Cabot, W. H., "A Dynamic Subgrid-Scale Eddy Viscosity Model," *Physics of Fluids A*, Vol. 3, July 1991, pp. 1760–1765.

[13]Girimaji, S. S., and Abdol-Hamid, K. S., "Partially-Averaged Navier Stokes Model for Turbulence: Implementation and Validation," AIAA Paper 2005-0502, Jan. 2005.

[14]Shih, T.-H., Chen, K.-H., and Liu, N.-S., "A Non-Linear k–ε Model for Turbulent Shear Flows," AIAA Paper 98-3983, July 1998.

[15]Shih, T.-H., Zhu, J., Liou, W. W., Chen, K.-H., Liu, N.-S., and Lumley, J. L., "Modeling of Turbulent Swirling Flows," NASA TM 113112, Aug. 1997.

[16]Shih, T.-H., Zhu, J., and Lumley, J. L., "A New Reynolds Stress Algebraic Equation Model," *Computational Methods in Applied Mechanical Engineering*, Vol. 125, No. 24, 1995, pp. 287–302.

[17]Tennekes, H., and Lumley, J. L., *A First Course in Turbulence*, MIT Press, 1972.

[18]Shih, T.-H., Liou, W. W., Shabbir, A., Yang, Z., and Zhu, J., "A New k–ε Eddy Viscosity Model for High Reynolds Number Turbulent Flows," *Computers and Fluids*, Vol. 24, No. 3, 1995, pp. 227–238.

[19]Chen, K.-H., Norris, A. T., Quealy, A., and Liu, N.-S., "Benchmark Test Cases for the National Combustion Code," AIAA Paper 98-3855, July 1998.

[20]Ajmani, K., and Chen, K.-H., "Unsteady Flow Computations for the NCC," AIAA Paper 2001-0972, Jan. 2001.

[21]Zagarola, M. V., and Smith, A. J., "Experiments in High Reynolds Number Turbulent Pipe Flow," *Physical Review Letters*, Vol. 78, 1997.

[22]Shih, T.-H., Povinelli, L. A., and Liu, N.-S., "Application of Generalized Wall Function for Complex Turbulent Flows," *Journal of Turbulence*, Vol. 4, April 2003, pp. 1–16.

[23]Den Toonder, J. M. J., "Drag Reduction by Polymer Additives in a Turbulent Pipe Flow: Laboratory and Numerical Results," Ph.D. Dissertation, Delft Univ. of Technology, Delft, The Netherlands, 1995.

[24]Kim, W.-W., Menon, S., and Mongia, H. C., "Large Eddy Simulation of Gas Turbine Combustor Flow," *Combustion Science and Technology*, Vol. 143, Aug. 1999, pp. 25–62.

F. Grinstein
Guest Editor